Geophysical Research Letters

Supporting Information for

Melting of the Chhota Shigri Glacier, Western Himalaya, Insensitive to Anthropogenic Emission Residues: Insights from Geochemical Evidence

S. Nizam[1], I. S. Sen[1], T. Shukla[1] and D. Selby[2, 3]

[1]Department of Earth Sciences, Indian Institute of Technology Kanpur, Kanpur, UP 208016, India.
[2]Department of Earth Sciences, University of Durham, Durham DH1 3LE, UK.
[3]State Key Laboratory of Geological Processes and Mineral Resources, School of Earth.

Contents of this file

Introduction

This supporting information provides brief notes on study area, engine exhaust sampling experiment, supplementary analytical details, and additional figures and tables to support results and discussion.

Text S1. Study Area

The majority of the western Himalayan glaciers have up to 19% of its surface area covered with debris (Brun et al., 2019). In contrast, the CSG has only 3.4% (lowest in the basin) of its surface area covered with debris (Vincent et al., 2013) and is therefore an excellent site to study long-distance emission inputs. The CSG (32.28° N, 77.58° E) is located in the Lahaul-Spiti valley, western Himalaya, India at an elevation between 4050 and 6263 m a.s.l. (Figure S1). The total axial length of the glacier is ca. 9 km and covers an area of ca.15.5 km^2. The equilibrium line of the CSG occurs at an altitude of ca. 4900 m a.s.l. (Wagnon et al., 2007). Presently, CSG has a total ice mass of ~1.57×10^{12} kg (after ice density 900 kg/m^3 and ice volume 1.74 km^{-3}) (Cogley, 2012; Ramsankaran et al., 2018) and has an ice mass wasting rate of 0.50 m $w.e.a^{-1}$ since the end of the last century (Azam et al., 2019). The meltwater feeds the Chandra River, which ultimately joins the Indus (Sindhu) river and provides water to an excess of 300 million people in the region of the Indus Basin.

Text S2. Geology and Meteorology of the Study Area

The CSG is surrounded and underlain by the late Proterozoic to early Cambrian age High Himalayan Crystalline Sequence (HHCS), which comprises highly metamorphosed granite-gneiss, schistose gneiss, augen gneiss, muscovite-biotite schist, quartzite, schist and low-grade metamorphic rocks (Kumar and Dobhal, 1997). Specifically, in the CSG catchment the glacial valley walls consist of mildly metamorphosed, intensely deformed fine-grained black slates, phyllites, and schists. The HHCS are often intruded by late Proterozoic to early Paleozoic mafic dykes, sills, and pegmatitic veins (Miller et al., 2001; Thakur & Patel, 2012; Thöni et al., 2012).

Meteorological data sets recorded within the glacier catchment divide the year into four seasons. These are, a warm summer monsoon (June to September), a cold winter (December to March), a pre-monsoon (April to May) and post-monsoon (October to November) period (Azam et al., 2014). Two principle atmospheric circulation patterns are prevalent over the CSG region; the southwest monsoon, which originates in the Arabian Sea and the Bay of Bengal during the summer from July through to September, and the Western Disturbances that originate in the Mediterranean Sea during winter from January through to April (Bookhagen & Burbank, 2010). The majority of the annual precipitation across the CSG region originates from Western Disturbances (79%), with the remaining 21% being derived from monsoon precipitation (Azam et al., 2019). Noteworthy is that the western disturbance brings heavy snowfall to the CSG region (e.g., average 6.3 mm w.e.d^{-1} was recorded between Dec 2012–Jan 2013), with only 0.5 mm w.e. d^{-1} average rainfall being derived from the southwest monsoon, resulting in the region being within the monsoon-arid transition zone (Azam et al., 2014). In addition to the two principle atmosphere circulation patterns, Hybrid Single Particle Lagrangian Integrated Trajectory Model (HYSPLIT) modeling results reveal 50% of the air mass that reaches the glaciers originates from the west, within ~250 km of the study site, while the remaining air masses being more long-range in origin (Nizam et al., 2020)

Text S3. Engine Exhaust Experiment

To obtain diesel engine exhaust particulates, engine experiments were performed in a contemporary common rail direct injection (CRDI) diesel engine (Tata; Safari DICOR 3.0 L) coupled with an eddy current dynamometer. The experiments were conducted in the Engine Research Laboratory at the Indian Institute of Technology Kanpur, India by following published protocols (Agarwal et al., 2018). In brief, exhaust particulates were collected on a 47 mm quartz filter paper (PM2.5) that was fitted on the exhaust tail type of the CRDI diesel engine. The operating conditions of the engine were optimized to those types of vehicles driven in India (outlined in (Agarwal et al., 2018). To avoid the possibility of any contamination with previous experiments, the walls of the photochemical chamber were thoroughly cleaned using ethanol and high purity water (18.2 MΩ cm) from a Millipore water purification system, and before sampling, zero air supply (containing less than 0.1 ppm of total hydrocarbon) was used to flush the photochemical chamber thoroughly.

Text S4. Sample Preparation

To remove any moisture, all cryoconite and moraine samples were first dried at ~70 °C. Cryoconite sediments size varies from fine granule (≤3 mm) to clay-sized fraction (≤0.002 mm). Several handpicked rock particles (3-60 mm) from each moraine sample were collected to represent the local lithology (hereafter referred to as local rock). Moraine samples were sieved to obtain bulk (<3 mm) and fine (<63 μm) fractions for geochemical analysis. The fine fraction serves as a proxy of any wind-blown material (Pye, 1995; Shao, 2009), whereas, the bulk fraction represents the local rocks as stated above. Bulk cryoconite (20-50 g), moraine (10-15 g fine fraction, 100 g bulk), local rock (100 g), and coal (100 g) samples were grounded to a homogeneous powder (20 μm) in an agate mill for major and trace elemental (details in Text S5) and Re-Os analysis.

Text S5. Major and Trace Element Analysis

Major elements for the cryoconite, fine, and bulk moraine size fractions were measured with a Wavelength Dispersive X-Ray Fluorescence spectrometer (Rigaku ZSX Primus II) at the Indian Institute of Technology, Kanpur, India. Oxide abundances were determined from sample powders that were fused with lithium tetra borate mixed with lithium bromide ($Li_2B_4O_7$-$LiBO_2$-LMR) flux (1:10 ratio) in a Pt crucible at 1800 °C for 30 minutes to form fused glass beads. The reference standard SDTSD-4 (stream sediment) from Canadian Certified Reference Material Projects was used as a calibration standard. Loss on ignition (LOI) was determined by heating 1 g sample in an oven from 100 to 1000 °C. A combination of NIST SRM 2709a (San Joaquin soil) and NIST SRM-8704 (Buffalo River sediment) from the USGS was used to assess the data quality. The measured values of the reference materials were within the uncertainty of the certified values (Table S1).

Trace metal and Rare Earth Element (REE) concentration analyses were performed at the Indian Institute of Technology Kanpur, India on an Agilent Triple Quadrupole Inductively Coupled Plasma Mass Spectrometer (QQQ-ICP-MS). Approximately 100 mg of sample powder was digested in pre-cleaned Teflon beakers at 150± 5 °C using a 2 mL mixture of HF: HNO_3 (4:1) for 48 hours. After digestion, the samples were dried and re-dissolved in aqua regia for 24 hours. To remove any organic materials, the cryoconite samples were further digested in 2 mL of ultra-clean HNO_3 for 24 hours at 130˚C. The digested samples were slowly evaporated to dryness at 100 °C, and if required, acid digestion steps were repeated for incomplete digestion. Trace element concentrations were determined from ~350 ppm total dissolved solid solutions. Three procedural blanks, and three Reference Material GS-N (granite), GeoPT28 (shale) and SRM-2704 (river sediment) were also digested following the same procedures. All samples and standards were spiked with ~5 ppb Rh internal standard solution to monitor and correct any drift in intensities due to matrix/drift effects. The instrument was run both in He and O_2 gas reaction mode to optimize the separation of measured isotopes from polyatomic interferences. Sample duplicates show reproducibility within 5% for most of the elements (Table S2). The final concentrations are all blank corrected using the average procedural blank concentrations. Average blank corrections were less than 1% for the majority of the elements. The measured trace element concentrations are in agreement with the reference materials (Table S2 and S3).

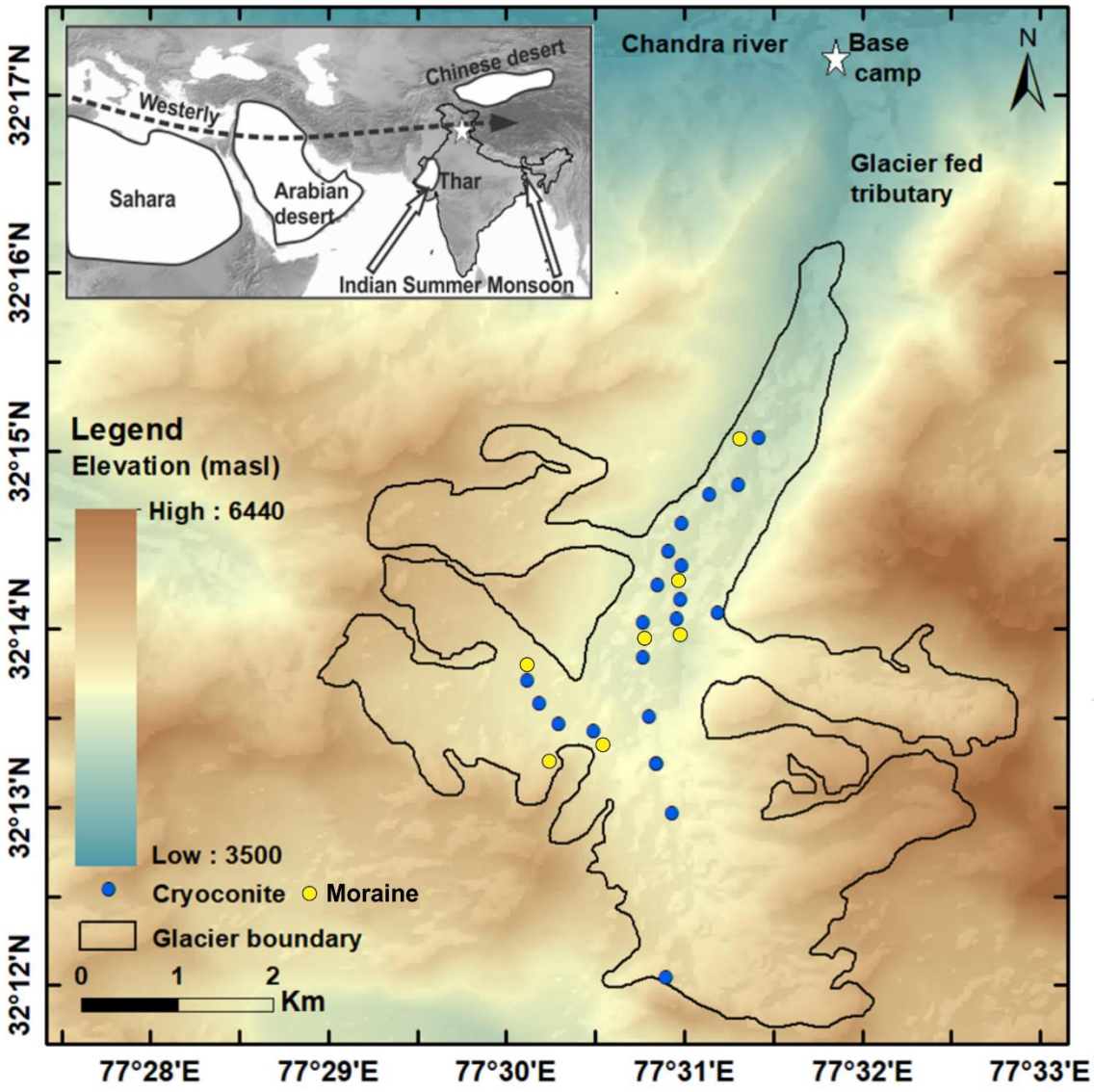

111

112 **Figure S1.** Map showing geographical location and cryoconite and moraine sampling points
113 along the ablation zone of the CSG. Inset figure shows regional atmospheric circulation patterns
114 in the glacier valley and desert distribution traced after (Parsons & Abrahams, 2009).

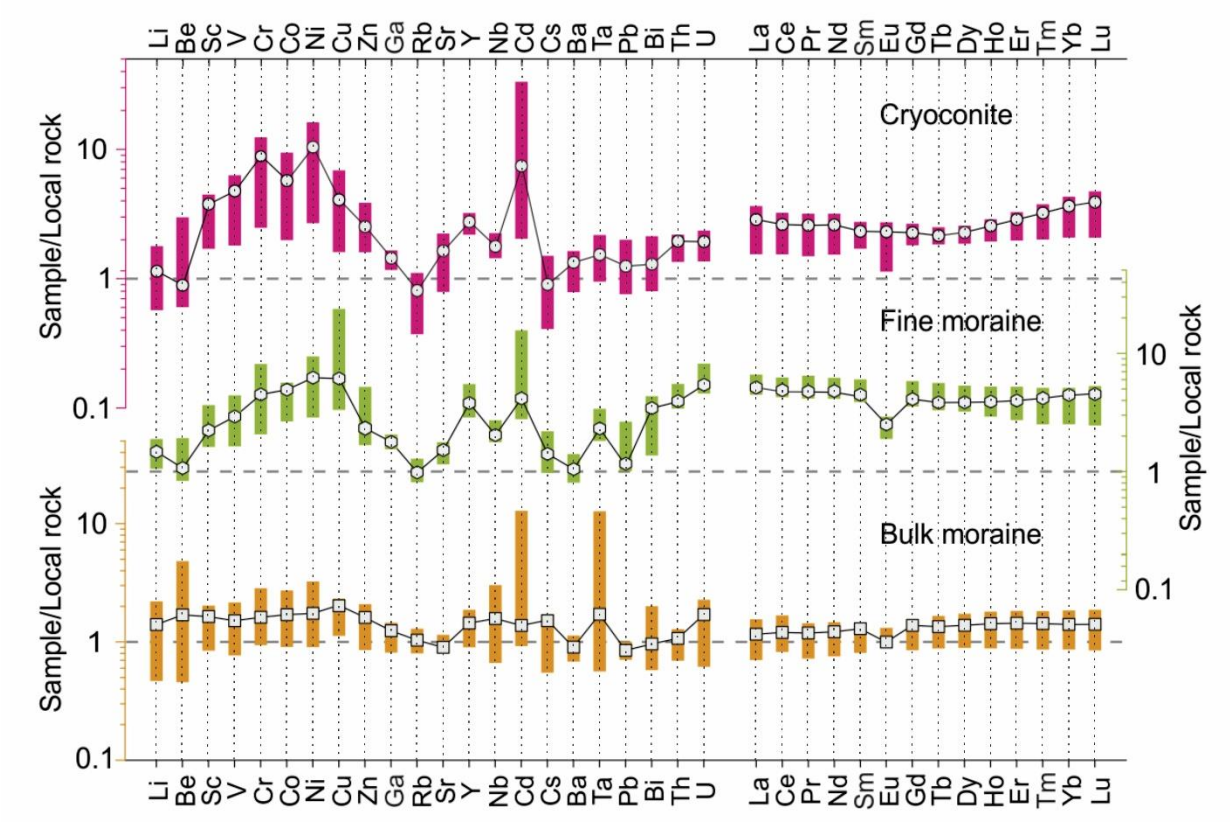

Figure S2. Local rock normalized elemental patterns for supraglacial cryoconite and moraine. Trace metal and rare earth elements are arranged in increasing atomic number. The upper and lower end of the bars represent the minimum and maximum values, the open symbol within the bar is the median value. Dashed straight line passing through unity is average local rock composition and any deviation from this line reflects additional source input or mineral sorting and elemental mobility attributed to physical weathering and transportation processes.

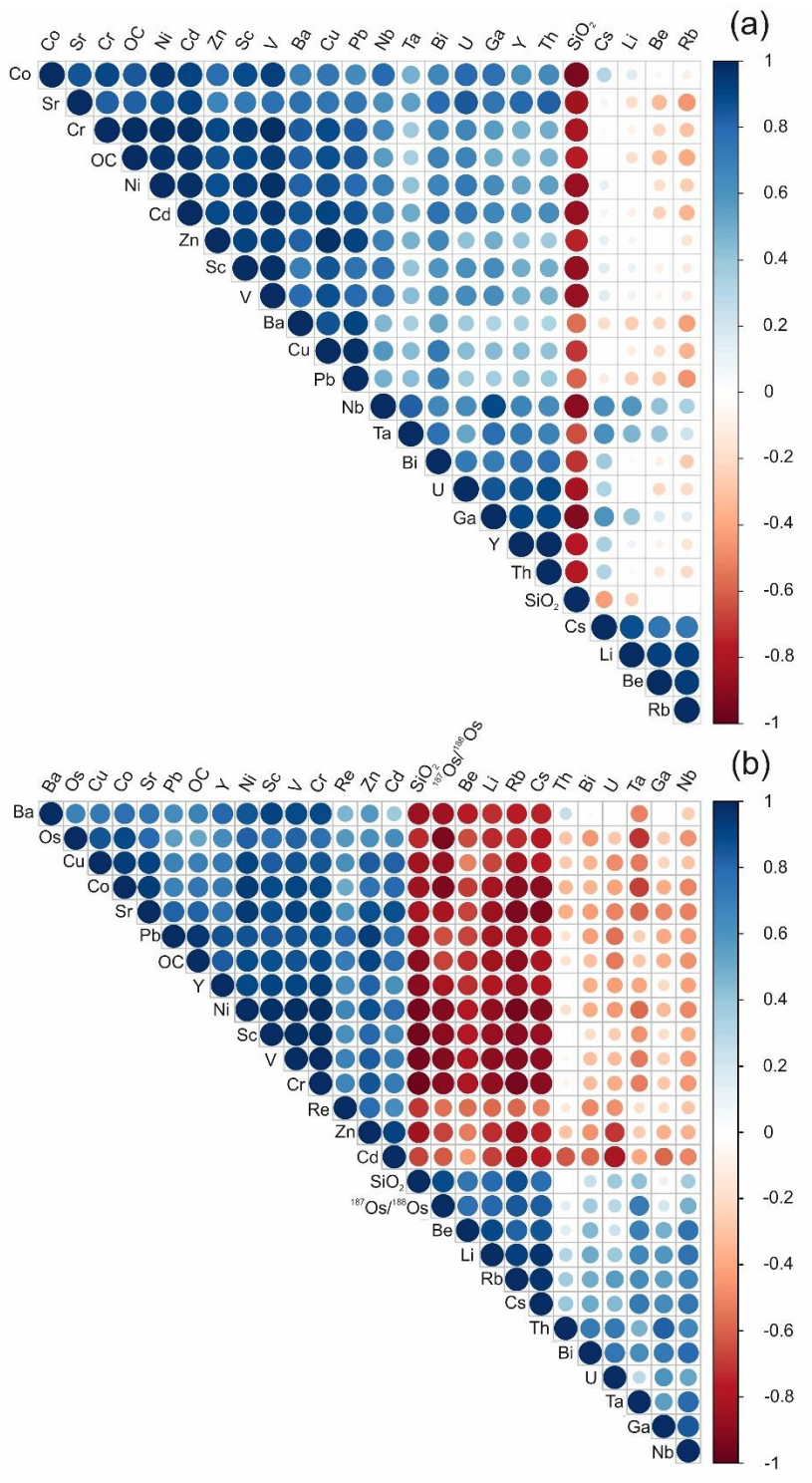

122

123 **Figure S3.** Correlogram showing Pearson correlation between trace metal, SiO_2, Re-Os, and
124 $^{187}Os/^{188}Os$ for (a) moraine (b) cryoconite. Positive correlations are displayed in blue and negative
125 correlations in red color. The color intensity and the size of the circle are proportional to the
126 correlation coefficients.

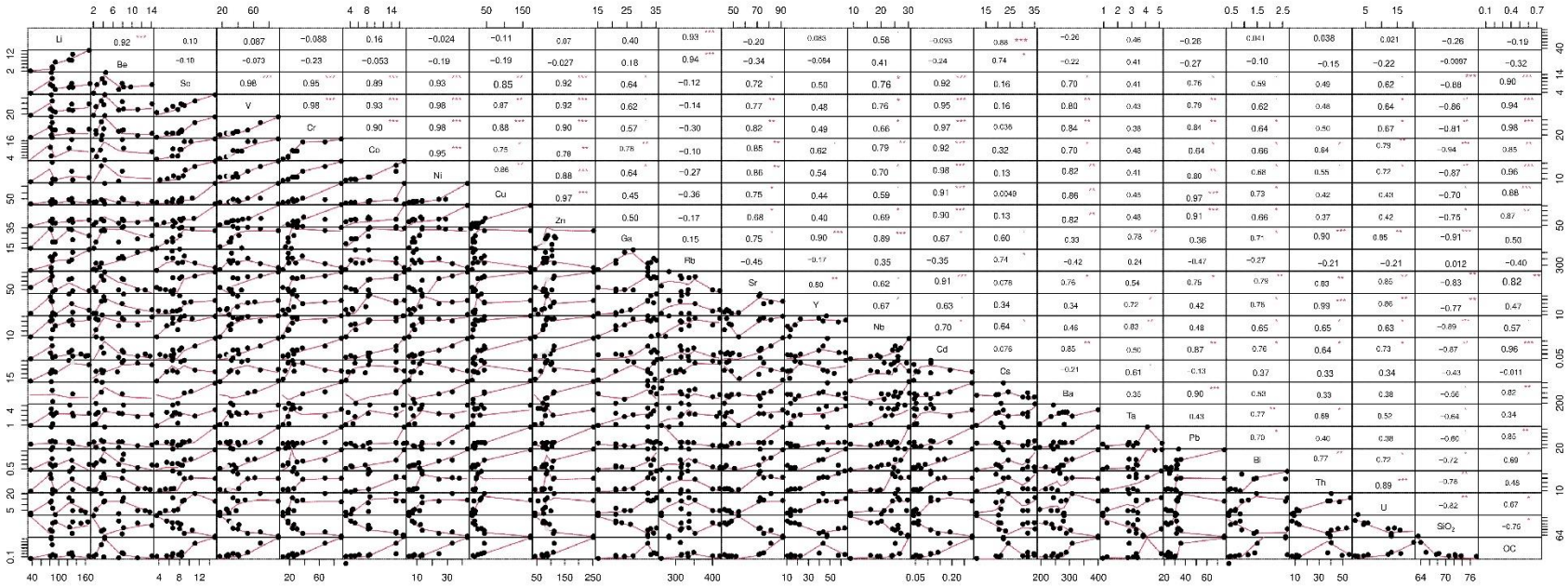

Figure S4. Distribution plot for each variable associated with trace metal and major oxides of moraine samples. On the bottom of the diagonal: the bivariate scatter plots with a fitted line are displayed. At the top of the diagonal: the value of the correlation plus the significance level as stars. Each significance level is associated to a symbol "***", "**", "*", ".", " " and associated p-values are 0.001, 0.01, 0.05, 0.1, 1) respectively.

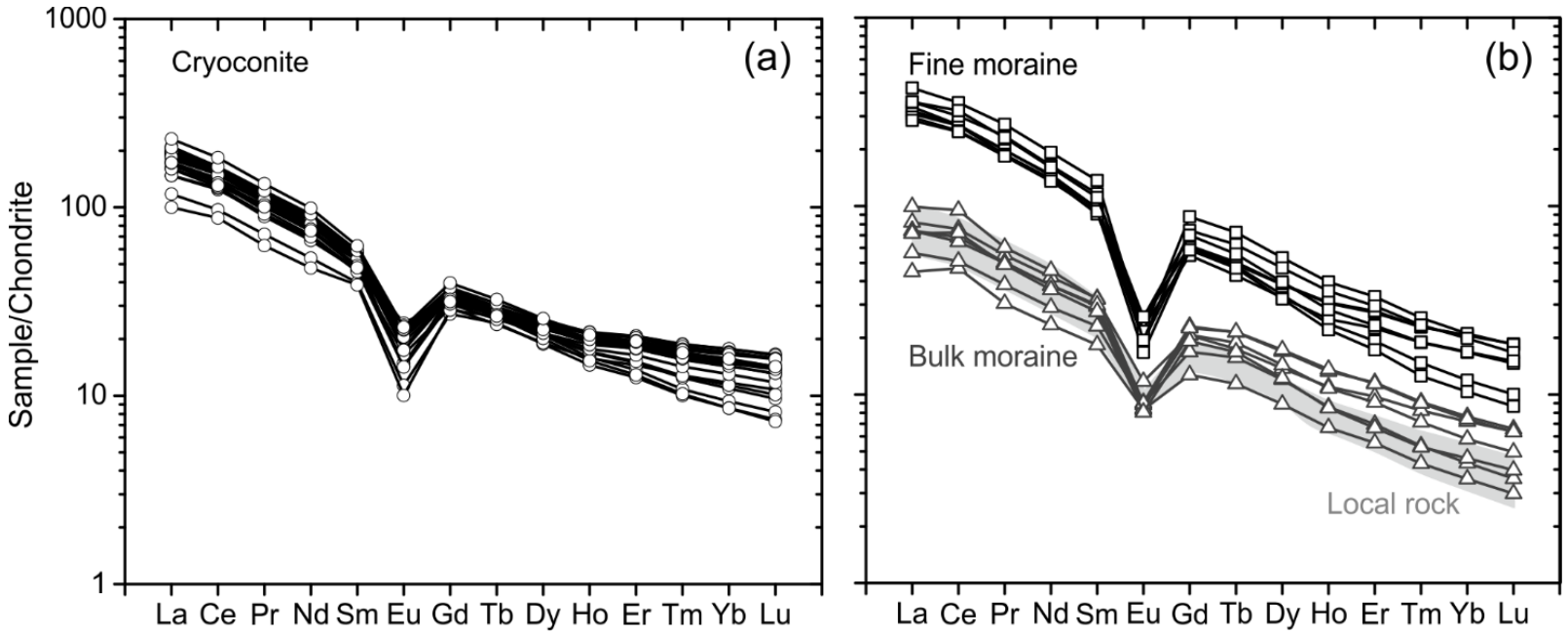

Figure S5. Chondrite normalized (McDonough and Sun, 1995) REE plots for individual cryoconite (a) and moraine debris (b) samples from ablation zone of CSG. Cryoconite samples showed negative EU anomaly of magnitude between local rocks and fine moraine fractions indicating local or geogenic origin.

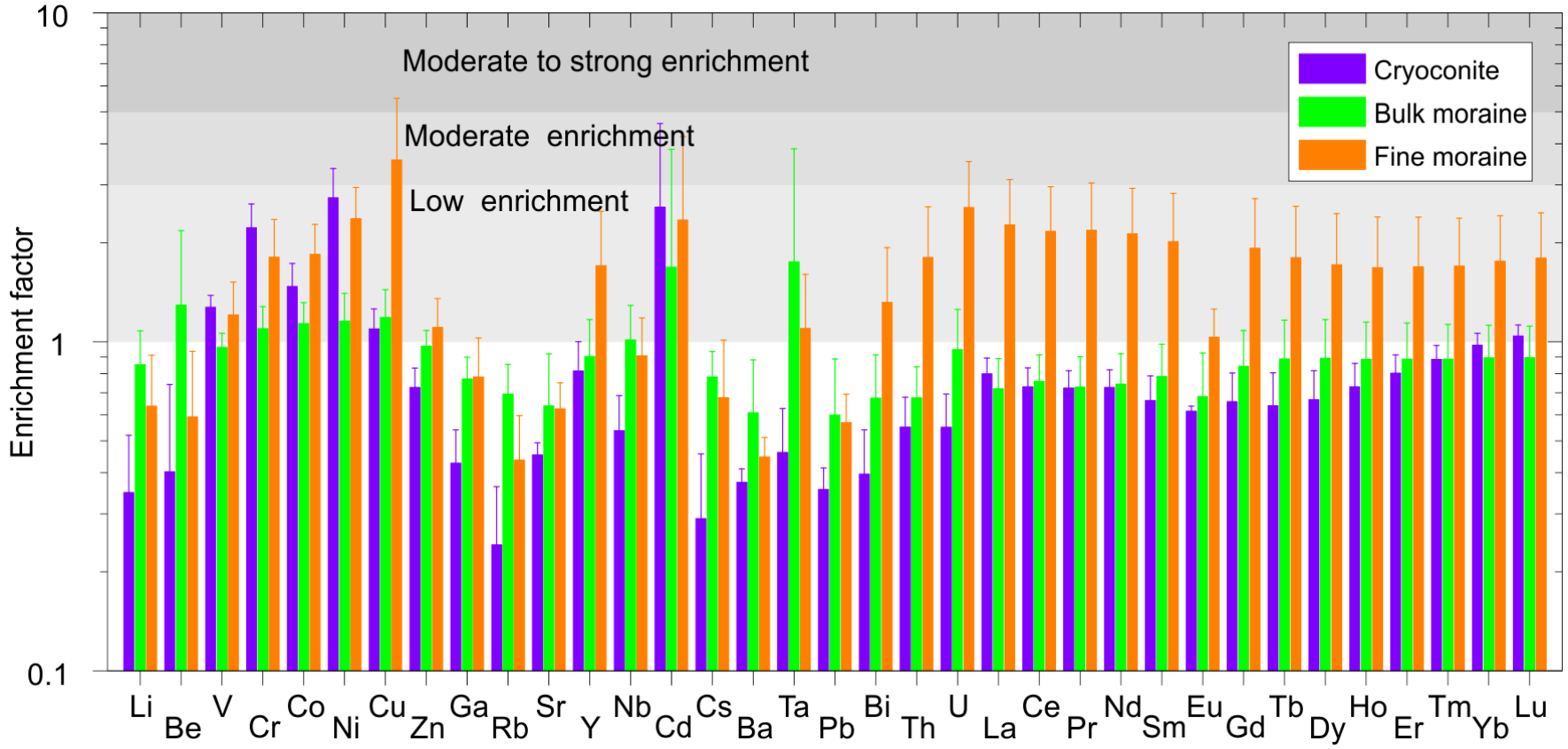

Figure S6. Enrichment Factor (EF) for trace metal and rare earth element in cryoconite (n=20, 1 SD), moraine (n=7, 1 SD) debris collected from CSG. EF (as $(X/Sc)_{sample}/(X/Sc)_{LR}$ for element X is calculated using Sc in local rock: LR (>3mm) (Barbieri, 2016).The EF value ≤1 corresponds to exclusively natural origin and EF value 1-3, 3-5, and 5-10 suggests low, moderate, and strong enrichment respectively.

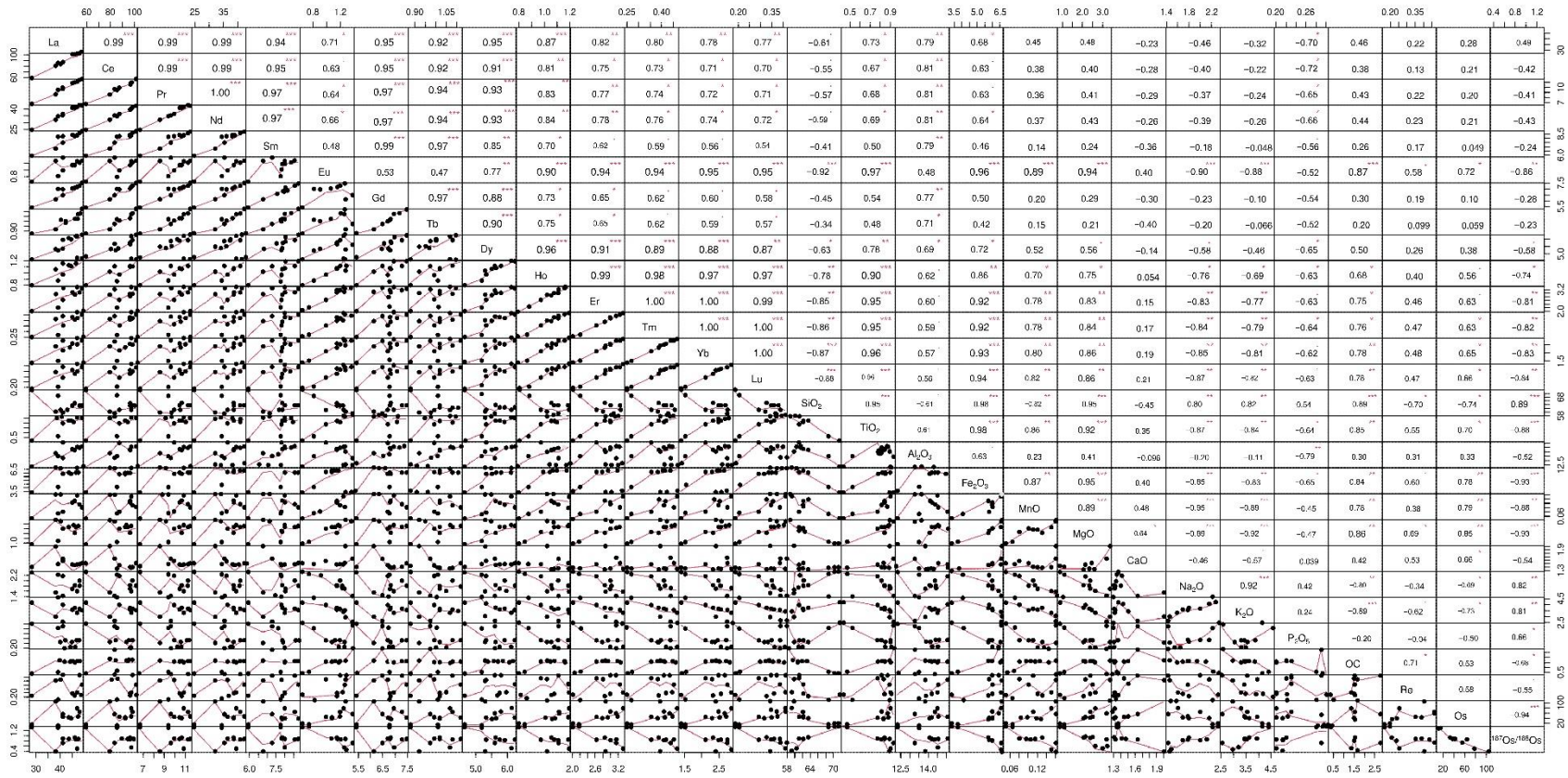

142

143 **Figure S7.** Distribution plot for each variable associated with REE, SiO_2, TOC, Re-Os concentration and $^{187}Os/^{188}Os$ ratio of cryoconite sample.

144 At the top of the diagonal: the value of the correlation plus the significance level as stars. Each significance level is associated to a symbol

145 "***", "**", "*", ".", " "and associated p-values are.001,.01,.05, .1, 1) respectively.

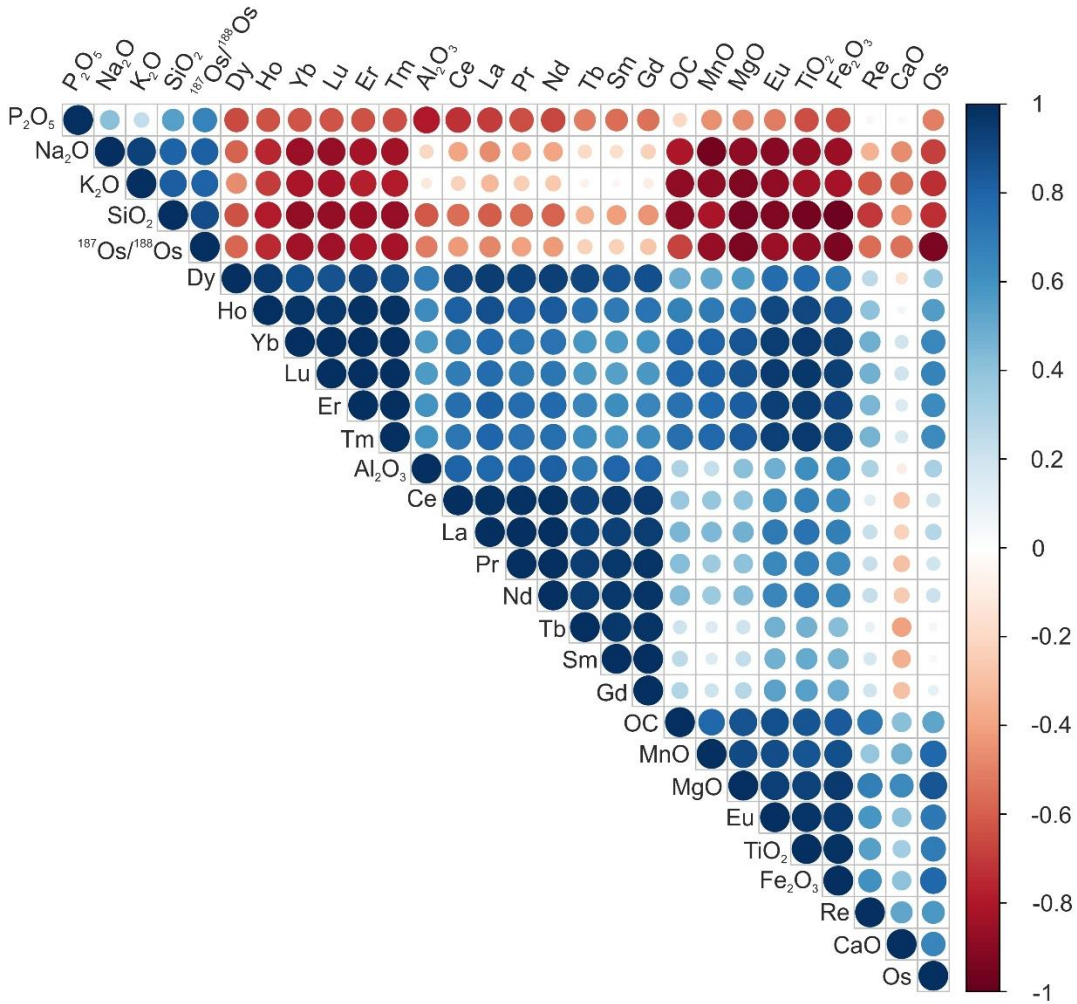

Figure S8. Correlogram showing Pearson correlation coefficient between REE and major oxide analyzed in cryoconite samples. Positive correlations are displayed in blue and negative correlations in red color. Color intensity and the size of the circle are proportional to the correlation coefficient

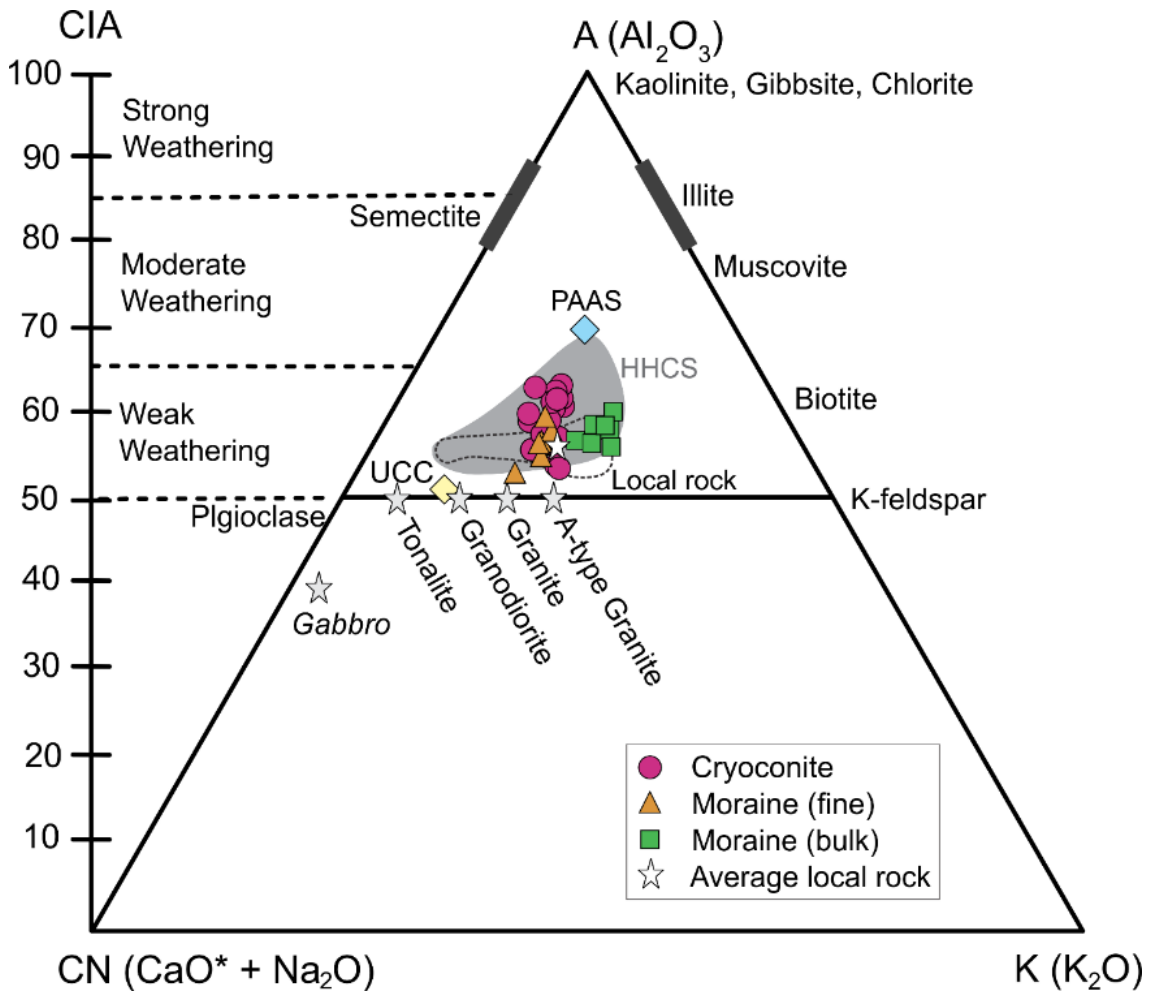

Figure S9. A-CN-K plot for supraglacial cryoconite, moraine, local granitoid rock, higher Himalayan Crystalline Sequence (HHCS), UCC, and PAAS. The vertical solid line plotted with a 10-unit interval represents weathering trends. Highly weathered sediments will move towards clay fraction end. The oxides abundance is in molar mass fraction and CaO* represents only the silicate fractions and determined by using the methodology described in an earlier study (Mclennan, 1993). Data source: Local rock (Maibam et al., 2016), HHCS (Richards et al., 2005), PAAS (Taylor & McLennan, 1985), and UCC (Rudnick & Gao, 2014).

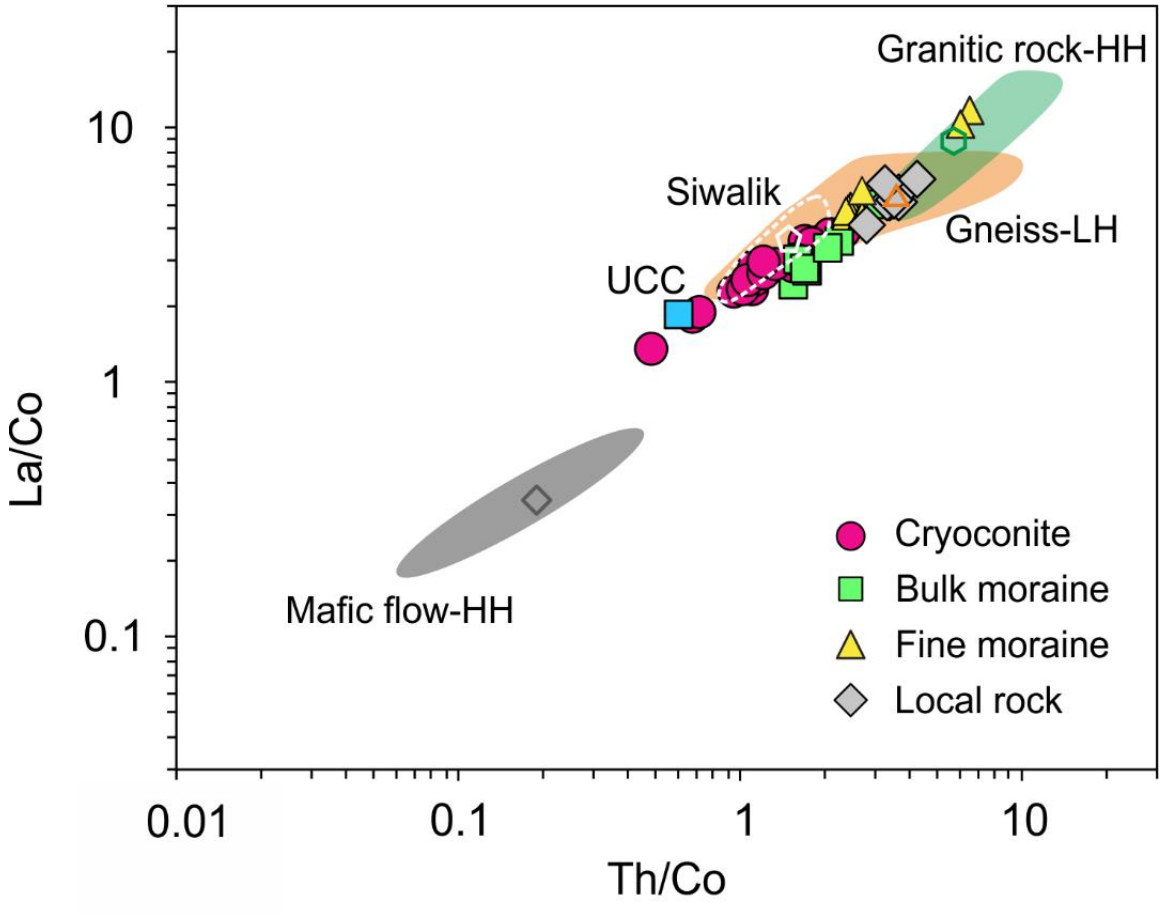

158

159 **Figure S10.** Bivariate concentration ratios plot of Th/Co versus La/Co showing cryoconite and
160 moraine signature compared to different rock units and UCC. The open symbols are average
161 values of lithology plotted as field abbreviations LH and HH refer to Lower Himalaya and Higher
162 Himalaya respectively. Data source: granitic and mafic rocks (Miller et al., 2001), gneiss (Islam et
163 al., 2011), Siwalik: clastic rocks (Ranjan & Banerjee, 2009) and UCC (Rudnick & Gao, 2014).

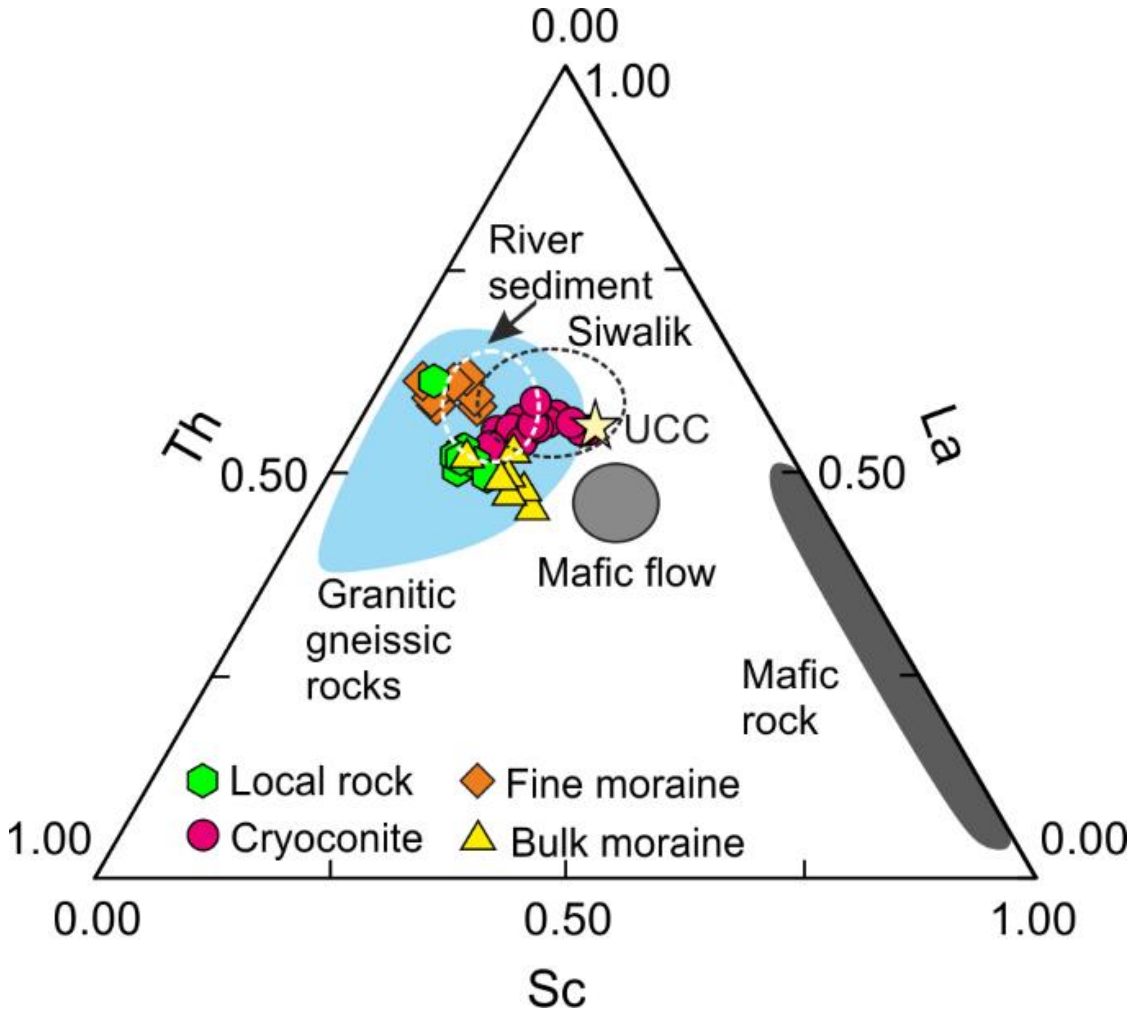

Figure S11. Ternary Th-Sc-La diagram illustrating lithological control on the composition of cryoconite and moraine debris. Fields of different rock types traced after published literature mentioned in Figure S10 except for mafic rocks (Srivastava & Sahai, 2001), and river sediments (Alizai et al., 2011).

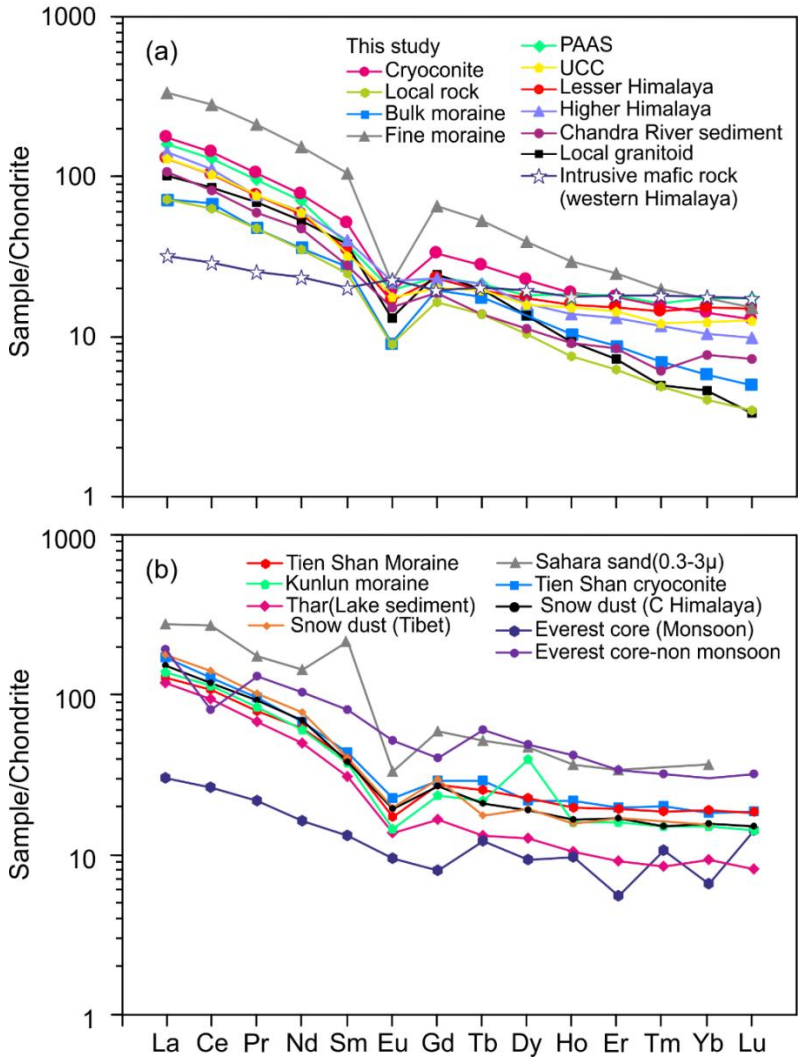

Figure S12. Comparison of chondrite normalized (McDonough and Sun, 1995) REE pattern of cryoconite and moraine with (a) local rock and sediment (b) snow dust, glacial moraine, sand and soil from other Himalayan regions and the Thar and Sahara deserts. Data source: (a) local granitoid (Maibam et al., 2016), Lesser Himalayan sediment (Das & Haake, 2003), Higher Himalaya (river sediment (Panwar et al., 2017), PAAS (Taylor & McLennan, 1985), intrusive mafic rock (Srivastava & Samal, 2019) and UCC (Rudnick & Gao, 2014); (b) Chinese glacial moraine cryoconite (Chang et al., 2000; Li et al., 2011), Glacial dust from Tibet and Nepal (Li et al., 2012) and Everest ice core dust (Zhang et al., 2009), Thar (Ferrat et al., 2011; Roy & Smykatz-Kloss, 2007) and Sahara sand (Castillo et al., 2008).

Table S1. Major element abundance in cryoconite (Cx) and selected moraine samples (Fine fraction: DF:<63 μ, Bulk fraction: DB:<3 mm).

Sample id	Elevation	SiO_2	TiO_2	Al_2O_3	Fe_2O_3	MnO	MgO	CaO	Na_2O	K_2O	P_2O_5	LOI	Total
	m a.s.l.	wt%	wt%	wt%	wt%	wt%	wt%	wt%	wt%	wt%	wt%	wt%	wt%
C1	4515± 2	63.4	0.84	14.06	5.71	0.13	2.03	1.3	1.79	3.62	0.22	6.79	99.9
C2	4582± 2	65.5	0.74	13.76	5.11	0.08	1.72	1.38	2.46	3.92	0.23	4.58	99.43
C3	4595± 3	68.6	0.52	13.48	4.05	0.07	1.08	1.34	2.21	4.54	0.28	3.27	99.42
C4	4649± 3	67.9	0.64	13.44	4.61	0.07	1.56	1.52	2.21	3.89	0.32	3.27	99.43
C5	4665± 2	71.4	0.43	12.3	3.32	0.05	0.86	1.36	2.31	4.14	0.3	2	98.45
C6	4683± 2	64.8	0.71	14.11	5.02	0.1	1.81	1.41	2.6	3.93	0.19	4.5	99.13
C7	4695± 3	67.1	0.64	13.43	4.76	0.08	1.54	1.44	2.06	3.97	0.29	3.9	99.19
C8	4701± 3	61.8	0.79	14.09	5.8	0.14	2.19	1.3	2.94	3.81	0.21	6.03	99.05
C9	4715± 3	62.1	0.84	14.18	5.98	0.12	2.36	1.32	1.68	3.47	0.2	7.09	99.37
C10	4738± 3	72.8	0.4	12.16	3.08	0.05	0.79	1.45	2.24	4.22	0.39	1.69	99.31
C11	4747± 3	61	0.9	14.49	6.54	0.15	2.62	1.31	1.58	3.29	0.2	6.98	99.04
C12	4750± 3	58.8	0.98	14.94	6.35	0.06	3.02	1.33	2.87	3.39	0.22	7.29	99.2
C13	4778± 3	62	0.81	14.35	5.96	0.11	2.37	1.33	1.99	3.54	0.23	7.2	99.9
C14	4816± 3	61	0.77	15.05	5.76	0.08	2.13	1.44	2.15	3.94	0.23	6.38	98.92
C15	4831± 3	60.7	0.91	14.74	6.46	0.11	2.71	1.42	1.69	3.35	0.21	7.4	99.65
C16	4871± 3	62.7	0.79	14.58	5.41	0.09	2.04	1.55	2.04	3.74	0.23	6.54	99.75
C17	4877± 3	62.1	0.89	14.54	5.99	0.1	2.49	1.5	1.77	3.42	0.23	6.87	99.86
C18	4908± 3	59.7	0.89	13.82	6.59	0.16	3.35	2	1.55	2.96	0.22	8.69	99.92
C19	4914± 3	58.5	0.93	13.25	6.55	0.16	3.18	1.63	1.42	2.54	0.29	10.56	98.98
C20	4928± 3	63.5	1.01	14.97	6.51	0.13	2.44	1.49	1.76	3.57	0.23	3.79	99.38
DF6	4556± 4	63.2	0.88	15.1	6.04	0.08	2.04	1.57	2.27	3.76	0.3	4.48	99.75
DF8	4657± 6	65.1	0.55	16.31	4.53	0.09	1.16	1.65	3.15	4.53	0.38	2.36	99.83
DF10	4715± 3	63.6	0.73	15.09	5.54	0.11	1.7	1.51	2.45	4.22	0.27	3.54	98.79
DF12	4751± 3	68.2	0.41	15.42	3.41	0.06	0.76	1.79	3.83	4.37	0.47	1.69	100.37
DF14	4823± 2	63.4	0.52	17.29	4.57	0.09	1.06	1.53	3.45	4.85	0.35	2.85	99.96
DF16	4890± 3	67.6	0.46	15.85	3.26	0.05	0.77	1.61	3.28	4.79	0.38	1.77	99.79
DF18	4928± 2	66.1	0.73	14.31	5.11	0.09	1.51	1.58	2.54	3.99	0.32	3.28	99.53
DB6	4556± 4	73.7	0.27	13.9	2.21	0.04	0.49	0.74	2.17	4.62	0.19	0.54	98.88
DB8	4657± 6	70.7	0.47	13.7	3.89	0.07	0.81	0.82	1.93	5.02	0.26	1.38	99.04
DB10	4715± 3	70.9	0.44	14.5	3.54	0.06	0.9	0.9	2.66	4.76	0.21	1.22	100.05
DB12	4751± 3	72.3	0.35	13.49	2.86	0.04	0.59	0.78	2.37	4.84	0.24	1.07	98.96
DB14	4823± 2	72.1	0.34	13.59	2.9	0.05	0.6	0.8	1.95	4.77	0.27	1.21	98.54
DB16	4890± 3	77.4	0.17	11.59	1.36	0.02	0.26	0.71	1.81	4.61	0.24	0.61	98.74
DB18	4928± 2	72.2	0.36	14.14	3.07	0.05	0.63	0.76	1.79	4.84	0.25	1.37	99.42
NIST reference material													
SRM 2709a[M]		63.9	0.57	13.34	4.95	0.07	2.47	2.84	1.67	2.52	0.17	7.8	99.15
		±0.73	±0.01	±0.82	±0.21	±0.00	±0.06	±0.24	±0.04	±0.03	±0.01	±0.01	
SRM 2709a[C]		59.6-	0.56-	14.06-	0.005-	0.06-	2.34-	2.65-	1.70-	2.41-	0.15-		93.61

	64	0.65	14.66	5.85	0.08	4.18	3.53	1.74	2.54	0.31		
SRM 8704^{M}	61.9	0.78	11.24	6.06	0.08	2.18	3.82±	0.97	2.44	0.23	10.04	99.59
	±0.01	±0.01	±0.41	±0.12	±0.001	±0.09	0.08	±0.13	±0.01	±0.01	±0.01	
SRM 8704^{R}	61.9-	0.71-	10.96-	5.62-	0.07-	1.90-	3.69-	0.71-	2.42-	0.20-		99.53
	62.2	0.78	13.74	6.02	0.08	2.14	3.83	0.78	2.57	0.22		

Note: Superscripts M refers to measured and C corresponds consensus values (http://georem.mpch-mainz.gwdg.de/sample_query.asp).

182

Table S2. Trace metal concentration (in ppm) in cryoconite and moraine samples. Cryoconite (Cx), local rocks (DB3-x, > 3 mm), moraine bulk fraction (DB-x, <3 mm), fine moraine (DF-x, <63 µm). Samples marked with apostrophe (') are duplicate analysis.

Sample	C1	C2	C3	C4	C5	C6	C7	C8	C9	C10	C11	GeoPT28^{M}	GeoPT28^{C}
Element												(n=3, 1 SD)	
Li	86	87	135	91	111	87	103	89	72	96	64	161± 17	164± 3
Be	3.9	5.7	12	8.5	6.5	9.7	6.5	4.3	3.2	9.8	3.1	3.29± 0.33	3.19± 0.08
Sc	15	13	11	11	8.7	12	10	15	15	6.9	17	24± 0.4	20± 0.2
V	93	80	60	67	47	76	64	93	100	37	116	250± 8	220± 1
Cr	90	71	46	56	32	66	53	88	98	27	115	117± 5	109± 1
Co	18	13	10	9.9	7.3	13	10	18	18	6.1	21	24± 0.8	23± 0.3
Ni	46	34	23	28	15	35	26	44	51	12	60	86± 3.1	83± 0.8
Cu	26	22	24	19	13	21	18	27	28	12	33	30± 1.2	31 ± 0.6
Zn	113	103	110	93	89	96	96	115	120	79	128	197± 7.1	187± 1.7
Ga	27	26	30	25	24	26	25	26	27	23	27	32 ± 0.8	27± 0.3
Rb	248	285	359	304	337	282	296	268	228	300	211	154± 6	147± 1.1
Sr	81	72	65	68	57	70	63	77	83	41	89	196± 4.7	178 ± 1.4
Y	30	32	27	31	26	25	33	31	32	29	36	36± 3.4	37± 0.3
Nb	25	24	30	23	22	25	23	24	22	19	23	19± 3.2	15 ± 0.2
Cd	0.25	0.14	0.21	0.11	0.08	0.19	0.14	0.24	0.32	0.08	0.35	0.4± 0.01	0.4± 0.19
Cs	17	20	29	22	24	18	23	22	16	24	13	7.9± 0.15	8.2± 0.1
Ba	379	375	288	337	243	374	294	380	400	224	407	772± 18	788± 8
Ta	2.7	2.4	3.4	2.3	2.4	3.4	2.5	2.2	1.9	1.9	2	2.4 ± 0.95	1.1± 0.03
Pb	35	30	28	25	26	29	28	37	38	23	40	31± 0.3	35± 0.3
Bi	1.38	1.1	1.3	0.82	0.57	0.76	0.75	0.97	0.85	0.77	0.81	0.59± 0.007	0.7± 0.02
Th	20	21	21	19	15	20	18	20	20	14	20	15± 0.04	16± 0.2
U	5.2	5.1	4.9	3.9	4.5	4.2	3.8	4.7	4.7	3.7	4.8	5.0± 0.12	5.76± 0.11

Note: Superscripts M and C correspond to measured and consensus values of GeoPT28 (http://georem.mpch-mainz.gwdg.de/sample_query.asp).

Table S2 continued

Sample Element	C11'	C 12	C13	C14	C15	C16	C17	C18	C19	C 19'	C20	SRM-2704^{M} (n=3, 1 SD)	SRM-2704^{C}
Li	64	73	70	106	85	108	87	64	43	49	85	40± 4.8	48
Be	2.8	3.1	3.1	5.3	3.3	4.4	3.6	3.1	2.5	2.6	3.1	1.76± 0.2	0.97-1.5
Sc	16	18	16	14	17	15	16	17	18	17	16	14± 0.4	12
V	108	126	113	90	112	96	110	124	129	119	103	103± 4.9	95± 4
Cr	107	116	102	89	111	98	113	123	136	127	102	135± 5.6	135± 5
Co	20	18	17	14	19	17	17	29	23	22	19	14± 0.4	14± 0.6
Ni	56	62	53	44	59	47	57	73	74	71	49	43± 1.3	44± 3
Cu	31	37	30	29	33	33	34	50	39	37	30	92± 2.6	99± 5
Zn	121	126	133	134	126	154	139	157	189	177	126	391± 9	438± 12
Ga	25	28	28	30	27	29	27	25	23	21	30	18± 0.4	15
Rb	197	218	263	280	212	280	223	168	129	120	261	102± 0.4	100
Sr	87	95	87	68	93	93	93	115	113	109	86	133± 6.4	130
Y	32	33	32	33	32	33	35	33	37	35	37	29± 3.8	27-33
Nb	22	25	25	26	22	26	25	22	21	19	27	15± 1.3	15
Cd	0.32	0.3	0.29	0.32	0.3	0.47	0.39	1.11	1.31	1.28	0.29	3.1± 0.04	3.5±0.22
Cs	13	14	17	24	14	21	16	10	8.1	7.9	18	5.5± 0.1	6
Ba	425	465	397	348	407	381	426	407	377	376	411	398± 19	414± 12
Ta	1.9	2.2	2.6	2.9	1.8	2.4	2.4	1.5	2.5	2.4	2.6	1.2± 0.3	0.97
Pb	40	38	45	39	43	53	43	42	60	61	37	138± 3	161± 17
Bi	0.95	0.91	0.95	0.89	0.81	0.96	0.89	0.56	0.52	0.64	0.67	0.5± 0.01	NA
Th	20	20	22	21	20	20	22	14	15	16	22	7.8± 0.08	9.2
U	4.8	4.8	5.3	4.3	4.9	4.8	4.7	4	3.4	3.3	5.8	3.03± 0.04	3.13± 0.13

Note: Superscripts M and C correspond to average measured and consensus values of NIST-2704 (http://georem.mpch-mainz.gwdg.de/sample_query.asp).

193 **Table S2 continued**

Sample Element	DB3-6	DB3-6'	DB3-8	DB3-10	DB3-12	DB3-14	DB3-16	DB3-18	*DB-6*	DB-8	DB-10	GS-N^{M} (n=3, 1SD)	GS-N^{C}
Li	67	79	78	93	74	91	40	73	*91*	167	106	56± 7	56± 8
Be	5	5.2	4.1	4.3	2.9	28	2.1	3.8	*7.1*	14	6.6	5.7± 0.5	5.4± 0.15
Sc	3.5	3.6	1.8	6.3	4.5	4.5	3.5	4.8	*5.4*	8.2	8	9.1± 0.3	7.3± 0.7
V	21	20	24	29	18	18	17	22	*28*	44	44	71± 3	65± 17
Cr	11	11	14	17	10	10	10	13	*17*	25	31	60± 2	55± 11
Co	2.9	2.9	3.5	4.7	2.8	3.2	2.4	3.7	*4*	8.3	8	76± 6	65± 11
Ni	4.3	4.2	5.6	7	4.2	4.9	3.6	5.4	*6.3*	12	15	37± 1.3	34± 11
Cu	7.4	7.4	7.1	6.4	5.1	10	7	7.9	*15*	17	16	20± o.7	20± 1.8
Zn	47	48	56	59	50	44	42	63	*72*	102	83	49± 1.5	48± 9
Ga	16	17	20	21	19	18	16	21	*21*	27	23	28± 1.3	22± 6.6
Rb	317	330	308	340	346	310	272	345	*335*	418	315	208± 12	185± 14
Sr	50	51	51	65	52	47	58	58	*48*	44	59	648± 30	570± 52
Y	12	12	13	14	10	11	10	12	*10*	22	17	15± 1.8	16± 12
Nb	13	13	13	13	13	12	8.9	13	*20*	26	40	27± 3.1	21± 4.5
Cd	0.03	0.03	0.79	0.04	0.06	0.04	0.03	0.04	*0.06*	0.07	0.51	0.06±0.002	0.04±0.012
Cs	19	19	17	28	24	20	11	20	*20*	30	31	5.5± 0.26	5.4± 0.5
Ba	278	280	302	368	234	287	337	248	*277*	256	321	1436± 83	1400± 124
Ta	1.5	1.6	1.9	1.3	1.6	1.5	0.8	1.7	*3.4*	3.1	20	3.4± 0.85	2.6± 0.36
Pb	31	31	28	30	30	29	32	32	*31*	23	27	45± 2.2	53± 9.2
Bi	0.72	0.75	0.44	0.93	0.4	0.57	0.3	2.56	*0.82*	0.45	1.31	0.20-0.07	0.18-0.57
Th	9.7	9.7	11	17	10	9	10	13	*7.1*	13	13	40± 2.3	41± 6.9
U	1.6	1.6	2.9	2.6	2.2	3.2	2.2	6.1	*1.5*	4.2	3	7.1± 0.42	7.5± 1.71

194 Note: Superscripts M and C correspond to average measured and consensus values of GS-N (http://georem.mpch-
195 mainz.gwdg.de/sample_query.asp).

196 **Table S2 continued**

Sample Element	DB-12	DB-14	DB-16	DB-18	DF-6	DF-6'	DF-8	DF-10	DF-12	DF-14	DF-16	DF-18
Li	130	129	35	85	82	100	128	143	122	138	80	84
Be	11	20	1.9	2.4	4.2	4	7.8	4.8	8.1	7.5	4	3.5
Sc	6.5	6.6	3.4	7.6	15	14	8.9	9.2	6.6	8	8.5	11
V	31	31	16	30	91	88	52	89	33	43	39	68
Cr	17	18	10	18	89	90	37	62	23	26	29	67
Co	5	6.4	2.8	5.2	17	16	15	15	8.6	15	8.2	15
Ni	7.1	8.8	4.2	8	43	42	24	35	13	21	13	33
Cu	11	17	8.2	11	170	166	42	46	34	50	24	42
Zn	79	80	42	70	251	246	107	122	85	117	82	110
Ga	24	25	15	21	32	31	34	33	35	36	33	32
Rb	399	380	259	313	280	262	351	322	334	415	314	311
Sr	46	44	54	42	91	88	75	82	72	59	71	81
Y	17	21	13	13	47	45	39	36	64	33	57	43
Nb	21	21	8.7	16	30	29	27	26	26	35	24	25
Cd	0.04	0.05	0.04	0.05	0.28	0.28	0.14	0.61	0.11	0.12	0.11	0.19
Cs	32	30	11	21	22	22	32	43	35	42	19	24
Ba	234	216	280	194	399	399	287	357	242	229	269	308
Ta	2.7	2.6	0.9	1.2	4.1	3.6	3.3	3.6	5.1	5.3	3.3	2.8
Pb	26	25	30	21	76	80	31	37	33	31	32	35
Bi	0.62	0.62	0.38	0.64	2.6	2.81	1.36	2.6	2.67	1.85	0.88	1.46
Th	11	11	8.8	11	39	40	37	36	56	40	49	40
U	4.4	4.7	2.4	5.6	13	13	13	11	16	18	12	20

197

198 **Table S3.** Rare earth element concentration (in ppm) in cryoconite and moraine samples. Sample
199 notions are same as Table 1 and Table 2 and apostrophe symbol refers to duplicate samples.

Sample / Element	La	Ce	Pr	Nd	Sm	Eu	Gd	Tb	Dy	Ho	Er	Tm	Yb	Lu
C1	46	96	10.6	38.3	7.82	1.141	6.8	1.016	5.61	1.051	2.84	0.385	2.31	0.324
C2	45	93	10.1	37.3	8.03	1.004	6.97	1.051	5.72	1.062	2.88	0.384	2.3	0.316
C3	39	85	9.34	34.2	7.73	0.806	6.75	1.007	5.17	0.871	2.19	0.267	1.5	0.202
C4	35	76	8.54	31	7	0.837	6.32	0.98	5.12	0.924	2.39	0.308	1.76	0.237
C5	28	59	6.67	24.6	5.9	0.638	5.4	0.877	4.63	0.795	2	0.248	1.38	0.184
C6	38	83	8.95	32.6	6.8	0.932	5.82	0.863	4.7	0.86	2.32	0.316	1.89	0.265
C7	35	78	8.3	30.5	6.89	0.8	6.17	0.97	5.2	0.935	2.43	0.315	1.83	0.249
C8	43	92	10.1	36.6	7.69	1.084	6.57	1.006	5.61	1.049	2.93	0.404	2.46	0.336
C9	45	96	10.4	38.4	7.97	1.142	6.77	1.016	5.74	1.073	2.98	0.417	2.54	0.357
C10	24	54	5.82	21.8	5.73	0.565	5.67	0.952	4.95	0.837	2.06	0.253	1.38	0.179
C11	47	97	10.8	39.2	7.96	1.238	6.93	1.065	6.11	1.189	3.32	0.465	2.84	0.408
C 11'	46	96	10.6	38.7	7.98	1.249	6.92	1.058	6.04	1.175	3.32	0.462	2.86	0.402
C 12	50	101	10.9	39.9	8.18	1.32	7.04	1.045	5.88	1.16	3.24	0.448	2.75	0.389
C 13	48	98	11.2	40.6	8.53	1.188	7.26	1.077	5.9	1.105	2.99	0.408	2.47	0.344
C 14	41	87	9.89	36.2	7.78	0.982	6.68	0.99	5.31	0.969	2.62	0.353	2.09	0.289
C 15	47	97	10.8	39.1	7.96	1.21	6.9	1.014	5.64	1.063	2.97	0.417	2.51	0.348
C 16	44	91	10.2	37.4	7.82	1.156	6.74	0.997	5.62	1.048	2.84	0.387	2.31	0.323
C 17	49	101	11.4	42	8.73	1.257	7.45	1.116	6.22	1.184	3.24	0.451	2.73	0.384
C 18	38	79	8.55	31.9	6.74	1.268	6.11	0.918	5.28	1.017	2.86	0.392	2.39	0.34
C 19	41	83	9.58	35.1	7.25	1.368	6.46	0.971	5.59	1.107	3.14	0.437	2.72	0.386
C 19'	41	80	9.34	34.4	7.08	1.33	6.29	0.955	5.53	1.086	3.08	0.431	2.66	0.384
C 20	55	113	12.4	45.2	9.24	1.299	7.9	1.171	6.31	1.148	3.11	0.417	2.53	0.35
DB3-6	15	35	3.76	13.9	3.3	0.477	2.92	0.464	2.43	0.414	1.04	0.129	0.7	0.091
DB3-6'	15	34	3.84	14.2	3.27	0.483	2.98	0.471	2.48	0.423	1.06	0.129	0.7	0.092
DB3-8	21	48	5.36	19.2	4.48	0.505	3.9	0.591	2.97	0.474	1.12	0.131	0.68	0.087
DB3-10	24	53	6.03	22.2	4.85	0.598	3.95	0.576	2.96	0.497	1.24	0.156	0.87	0.115
DB3-12	15	35	3.95	14.2	3.42	0.492	2.97	0.453	2.19	0.343	0.8	0.094	0.5	0.065
DB3-14	13	30	3.36	12.4	2.97	0.459	2.68	0.433	2.29	0.398	0.98	0.118	0.65	0.084
DB3-16	15	34	3.81	13.8	3.28	0.516	2.9	0.448	2.22	0.349	0.8	0.093	0.5	0.062
DB3-18	19	43	4.82	17.5	4.15	0.509	3.7	0.568	2.75	0.412	0.93	0.112	0.64	0.086
DB-6	11	29	2.82	10.7	2.71	0.468	2.53	0.412	2.19	0.364	0.89	0.106	0.57	0.073
DB-8	19	46	5.1	19.2	4.79	0.511	4.58	0.772	4.17	0.724	1.85	0.226	1.23	0.162
DB-10	24	58	5.6	20.8	4.74	0.66	4.1	0.63	3.39	0.6	1.56	0.203	1.16	0.157
DB-12	18	42	4.67	17.3	4.34	0.497	4.12	0.682	3.54	0.589	1.46	0.176	0.93	0.122
DB-14	18	40	4.63	17.4	4.43	0.477	4.49	0.777	4.25	0.743	1.82	0.222	1.19	0.156
DB-16	13	31	3.55	13.3	3.41	0.506	3.35	0.567	2.95	0.469	1.11	0.132	0.7	0.088
DB-18	17	44	4.54	16.5	4.07	0.454	3.82	0.607	3	0.463	1.06	0.13	0.74	0.098
DF-6	76	165	18.4	66.2	14.4	1.404	12.1	1.769	9.43	1.664	4.35	0.563	3.33	0.453

DF-6'	80	165	18.4	67	14.4	1.429	12.3	1.816	9.48	1.684	4.44	0.566	3.31	0.457
DF-8	73	164	17.5	63.7	14.4	1.08	12	1.737	8.31	1.299	3.08	0.364	1.92	0.246
DF-10	70	154	17.3	63.6	13.4	1.28	10.9	1.549	8.04	1.374	3.6	0.466	2.69	0.36
DF-12	100	217	25.2	88	20.2	1.216	17.5	2.619	13.1	2.16	5.29	0.631	3.39	0.453
DF-14	68	152	17.1	61.8	13.9	0.942	11.6	1.692	7.9	1.205	2.76	0.31	1.67	0.213
DF-16	84	184	21.8	74.9	17.2	1.094	14.8	2.255	11.6	1.931	4.72	0.577	3.2	0.411
DF-18	85	197	21.4	73.3	16.4	1.451	13.9	2.011	9.72	1.541	3.72	0.469	2.71	0.371
GeoPT28^{M}	51±	106±	12.1±	45±	9.1±	1.84±	7.8±	1.15±	6.5±	1.3±	3.7±	0.53±	3.38±	0.49±
	1.4	3.2	0.2	1.2	0.21	0.03	0.08	0.019	0.16	0.02	0.05	0.01	0.07	0.009
GeoPT28^{C}	53±	108.2±	12.6±	49.2±	9.62±	1.98±	8.54±	1.23±	7.1±	1.36±	3.79±	0.56±	3.64±	0.54±
	0.6	0.92	0.1	0.5	0.11	0.018	0.1	0.016	0.089	0.017	0.05	0.01	0.039	0.008
SRM-2704^{M}	30±	59±	7±	27±	5.5±	1.2±	5.3±	0.82±	5±	1.02±	2.96±	0.43±	2.72±	0.39±
	1.2	1.9	0.08	0.35	0.04	0.01	0.04	0.01	0.03	0.01	0.04	0.005	0.03	0.0002
SRM-2704^{C}	29	72	7.2	32	6.7	1.3	5.5	0.89	6	1.2	3.3	0.48	2.8	0.6
GS-N^{M}	75±	138±	14±	46±	7.1±	1.5±	4.8±	0.59±	3±	0.55±	1.5±	0.21±	1.35±	0.20±
	4.2	7.3	0.7	2.5	0.37	0.0.08	0.23	0.03	0.16	0.03	0.08	0.01	0.07	0.01
GS-N^{C}	75±	135±	14.5	49±	7.5±	1.7±	5.2±	0.6±	3.1±	0.68±	1.5±	0.22	1.4±	0.22±
	7.3	45.12		3.54	0.51	0.16	0.79	0.08	1.04	0.18	0.4		0.54	0.06

Note: Superscripts M and C correspond to average measured and consensus values of reference material mentioned in earlier tables.

Table S4. Calculated percent osmium contribution in cryoconite from individual sources: Local Moraine (LM), Less Radiogenic with low Os concentration mineral phase (LR) and Ultramafic Rock (UR).

Sample	LM	LR	UR
C1	66.7	31.8	1.5
C3	30.7	69.2	0.2
C5	40.7	59.1	0.2
C9	70.5	28.0	1.6
C11	69.9	24.1	6.1
C13	92.4	4.6	3.1
C14	74.4	23.5	2.1
C17	74.6	23.1	2.3